

https://dspace.org/

BaMn2P2: highest magnetic ordering temperature 122-pnictide compound

Jacobs, B. S.; Pandey, Abhishek

2023-04
American Physical Society
https://hdl.handle.net/10539/50014
Jacobs, B.S.; Pandey, A. BaMn2P2 : Highest magnetic ordering temperature 122-pnictide compound. Phys. Rev. Mater. 2023, 7, 044410, https://doi.org/10.1103/physrevmaterials.7.044410.

Downloaded from a DSpace repository. https://dspace.org/

$BaMn_2P_2$: Highest magnetic ordering temperature 122-pnictide compound

B. S. Jacobs [1,*] and Abhishek Pandey [2,3,†]

[1]Department of Physics, University of Johannesburg, Johannesburg 2006, Gauteng, South Africa
[2]Materials Physics Research Institute, School of Physics, University of the Witwatersrand, Johannesburg 2000, Gauteng, South Africa
[3]Department of Physics and Astronomy, Texas A&M University, College Station, Texas 77843, USA

(Received 22 February 2023; accepted 7 April 2023; published 21 April 2023)

We report the growth of high-quality single crystals of $ThCr_2Si_2$-type tetragonal $BaMn_2P_2$ and investigation of its structural, electrical transport, thermal, and magnetic properties. Our results of basal plane electrical resistivity and heat capacity measurements show that the compound has an insulating ground state with a small band gap. Anisotropic susceptibility $\chi_{ab,c}(T)$ data infer a collinear local-moment Néel-type antiferromagnetic (AFM) ground state below the ordering temperature $T_N = 795(15)$ K, which is highest among all the $ThCr_2Si_2$- and $CaAl_2Si_2$-type 122-pnictide compounds reported so far suggesting that the strength of magnetic exchange interactions is strongest in this material. The magnetic transition temperatures of $BaMn_2Pn_2$ (Pn = P, As, Sb, Bi) compounds exhibit a monotonic decrease with the increase of tetragonal unit cell parameters a and c, suggesting a strong dependence of the strength of the decisive magnetic exchange interactions on the separation between the localized spins residing on the Mn ions. The observed monotonic increase of both χ_{ab} and χ_c for $T > T_N$ suggests that short-range dynamic quasi-two-dimensional AFM correlations persist above the T_N up to the highest temperature of the measurements. The large T_N of $BaMn_2P_2$ demands for systematic hole-doping studies on this material as similar investigations on related $BaMn_2As_2$ with $T_N = 618$ K have led to the discovery of an outstanding ground state where AFM of localized Mn spins and itinerant half-metallic ferromagnetism with $T_c \approx 100$ K originating from the doped holes coexist together.

DOI: 10.1103/PhysRevMaterials.7.044410

I. INTRODUCTION

The search for new transition metals-based superconductors and their probable parent compounds got intensified after the discovery of high-temperature (high-T_c) superconductivity (SC) in iron-based layered pnictides and chalcogenides [1–5]. Specifically, after the discovery of SC in doped-$BaFe_2As_2$, significant efforts were put into the investigations of $ThCr_2Si_2$-type 122-tetragonal systems that crystallize with space group $I4/mmm$. The investigations carried out so far suggest that iron is an essential ingredient for achieving high-T_c SC within this family of compounds. On the other hand, exploratory efforts on related systems where in place of iron some other $3d$ or $4d$ transition metal ions constitute the metal-pnictide sublattice have led to quite interesting outcomes and ground states such as prototypical half-metallic behavior [6–8], spin-liquid phase embedded with antiferromagnetic (AFM) and ferromagnetic (FM) fluctuations [9–11], highly frustrated itinerant magnetism [12], low-temperature SC [13–16], discovery of new layered magnetic phases [17], large negative magnetoresistance (MR), and Anderson localization [18–20], to name a few.

Among the 122-type materials, Mn-based AMn_2Pn_2 (A = Ca, Sr, Ba, and Pn = P, As, Sb, Bi) semiconducting compounds have received special attention. Irrespective of the type of pnictide ion present, the Ca- and Sr-based AMn_2Pn_2 materials crystallize in $CaAl_2Si_2$-type trigonal structure with space group $P\bar{3}m1$ while the Ba-based compounds crystallize in $ThCr_2Si_2$-type tetragonal structure, suggesting that alkaline earth metals are the controlling factor for establishment of the ground-state crystal structure in these systems. Further, pnictide atoms control the unit-cell dimensions, hence, the separation between magnetic Mn ions [21,22]. As a result, with two accessible composition-based tunable control parameters, these systems offer immense opportunities for the investigation of structure-interactions-property relationship.

Specifically, small band gap semiconducting $BaMn_2Pn_2$ compounds with stacked-square-lattice of Mn ions undergo G-type AFM ordering with Néel temperature T_N considerably higher than room temperature (Table I). Interestingly, the most well-studied member of this family, $BaMn_2As_2$, undergoes insulator-to-metal transition by a small amount (<2%) of hole-doping [23] or by the application of moderate ~6 GPa pressure [24]. Unlike the related itinerant AFM spin-density wave compound $BaFe_2As_2$, where hole-doping leads to the formation of SC ground state [3–5], the higher levels of hole-doping ($\gtrsim$40%) results in stimulating prototype half-metallic behavior in $BaMn_2As_2$ [6–8].

In contrast to the thoroughly investigated As-, Sb-, and Bi-based counterparts [25–28], limited amount of experimental work has been reported on $BaMn_2P_2$. About two decades ago, Brock *et al.* performed magnetic susceptibility and neutron diffraction studies on a polycrystalline sample of $BaMn_2P_2$ and suggested that the material is a high-spin G-type

*sjacobs@uj.ac.za
†abhishek.pandey@wits.ac.za

 ©2023 American Physical Society

TABLE I. Structural and physical properties parameters of $BaMn_2Pn_2$ (Pn = P, As, Sb, Bi). All four compounds crystallize in $ThCr_2Si_2$-type tetragonal structure with space group $I4/mmm$ (SG: 221). The listed crystallographic parameters are the unit cell parameters a, c, c/a, z_{Pn}, and the distance between two nearest interlayer pnictogen atoms d_{Pn-Pn}. The listed physical properties parameters are Néel temperature T_N, Sommerfeld coefficient γ, coefficient β and δ of lattice heat capacity, Debye temperature Θ_D, and band gap Δ obtained from the resistivity measurements.

Parameter	$BaMn_2P_2$ (This paper)	$BaMn_2As_2$ Ref. [25]	$BaMn_2Sb_2$ Ref. [26]	$BaMn_2Bi_2$ Ref. [27]
Structure parameters				
a (Å)	4.0381(1)	4.1686(4)	4.397(4)	4.4902(3)
c (Å)	13.0653(3)	13.473(3)	14.33(2)	14.687(1)
c/a	3.2355(2)	3.232(1)	3.259(8)	3.2709(5)
z_{Pn}	0.3568(2)	0.3615(3)	0.3642(1)	0.3692(3)
d_{Pn-Pn} (Å)	3.742(5)	3.732(9)	3.89(1)	3.84(1)
Property parameters				
T_N (K)	795(15)	618(3)	450(10)	387.2(4)
γ (mJ/mol K^2)	0.9(9)	0.0(4)	0.02(4)	0
β (mJ/mol K^4)	0.23(3)	0.65(3)	0.680(3)	0.434(3)
δ (mJ/mol K^6)	0.0027(1)	0	0	0
Θ_D (K)	348(17)	246(4)	202(1)	165
Δ (meV)	24(2)	27 & 6.5	160 and 18	

antiferromagnet where Mn spins carry a moment of 4.2(1) μ_B and $T_N > 750$ K [29,30]. After their work, there was no further attempt to investigate the properties of this material. In this paper we report the single crystal growth as well as structural, electronic, magnetic, and thermal properties of $BaMn_2P_2$ and attempt to establish structure-property relationship within insulating $BaMn_2Pn_2$ compounds. We show that the value of T_N in $BaMn_2P_2$ is highest among the 122-pnictide compounds. Additionally, our results also establish a strong correlation of the value of T_N on intralayer as well as interlayer distance between the Mn ions.

II. EXPERIMENTAL DETAILS

Single crystals of $BaMn_2P_2$ were grown using solution growth technique in Sn flux using high purity starting elements Ba (99.99%), Mn (99.98%), P (99.999%), and Sn (99.999%) weighed in the molar ratio Ba:Mn:P:Sn = 1:2:2:45. The required amounts of the pure elements were placed in an alumina crucible and sealed inside a quartz tube under a partial Ar pressure of about 0.25 atm. The sealed tube was placed in a furnace and heated from room temperature to 400 °C in 10 h and held at this temperature for 30 h. The assembly was further heated to 1180 °C in 25 h and maintained at this temperature for 40 h. Further, it was slow-cooled to 700 °C in 130 h. At this temperature, the Sn flux was decanted [31] using a centrifuge and shiny plate-like crystals of $BaMn_2P_2$ of typical size of $2 \times 2 \times 0.5$ mm^3 were obtained. Room temperature powder x-ray diffraction (XRD) measurement was performed on a few small crushed crystals of $BaMn_2P_2$ using a Bruker D8 Advance Powder Diffractometer equipped with a Cu-K_α radiation source. Two-phase Rietveld refinement was performed using the FullPROF package [32].

Temperature T dependence of heat capacity C_p as well as four-probe basal ab-plane electrical resistivity ρ_{ab} measurements were done using a Physical Properties Measurement System (PPMS) of Quantum Design Inc. (QDI), USA. Single component silver-filled epoxy was used for making electrical contacts of platinum wires on the single crystal for electrical measurements. Temperature dependence of anisotropic magnetic susceptibilities $\chi_{ab,c}(T)$ were measured using two different options: for 2 K $\leqslant T \leqslant$ 400 K using a SQUID-Magnetic Properties Measurement System (MPMS) of QDI and for 350 K $\leqslant T \leqslant$ 850 K using the high-temperature Vibrating Sample Magnetometer (VSM) Option of a PPMS. Isothermal magnetization M versus applied field H at five different temperatures were measured using MPMS.

III. RESULTS

A. Crystal structure

The powder XRD data collected on a few crushed crystals of $BaMn_2P_2$ along with the two-phase Rietveld refinement fit, difference profile and Bragg positions are shown in Fig. 1. The two-phase Rietveld refinement was performed to include the reflections originating from the small amount of adventitious Sn flux remaining on the surface of the small crystals that were crushed to powder. The fitted values of the tetragonal lattice parameters a, c, and the c-axis phosphorus position parameter z_P of $BaMn_2P_2$ are listed in Table I along with the corresponding parameters of $BaMn_2As_2$, $BaMn_2Sb_2$, and $BaMn_2Bi_2$. Figures 2(a) and 2(b) show the variation of the lattice parameters a and c, respectively, of the four $BaMn_2Pn_2$ compounds with the type of pnictogen atom present in the unit cell. The results highlight a nearly linear increase in a and c as we go down in the group from P to Bi. Due to the linear variation in the lattice parameters, the c/a ratio of these materials

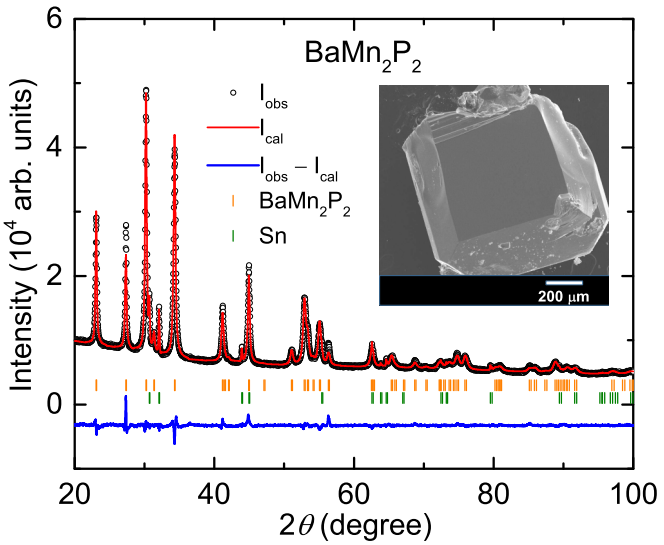


FIG. 1. Room temperature powder x-ray diffraction data collected on Sn-grown crushed crystals of $BaMn_2P_2$, two-phase Rietveld refinement profile, difference profile, and Bragg positions of $BaMn_2P_2$ as well as adventitious Sn. Inset: Scanning electron microscope image of a crystal of $BaMn_2P_2$.

stay nearly constant at a value of 3.25(2) (Table I). In contrast to the large variation of the a and c parameters, the distance between adjacent pnictogen layers $d_{Pn-Pn} = c(1 - 2z_{Pn})$ does not show any noteworthy dependence on the type of pnictogen present in the lattice and exhibits a nonmonotonic behavior with a mean value of 3.81(8) Å [Fig. 2(c)]. It is also important to highlight here that the intralayer distances between nearest (NN)- and next-nearest-neighbor (NNN) Mn spins are $a/\sqrt{2}$ and a, respectively, while the interlayer distance between the two adjacent Mn spins along the c axis is $c/2$.

B. Electrical transport

Figure 3 shows the ab-plane electrical resistivity ρ_{ab} of a single crystal of $BaMn_2P_2$ versus T for two different applied fields $\mu_0 H = 0$ and 7 T. The $\rho_{ab}(T)$ stays nearly constant and exhibits a small increase of about 10% with decreasing T from 300 K to ∼130 K [inset (a), Fig. 3]. However, there is a sharp rise in the $\rho_{ab}(T)$ values below 130 K where it shows a fourfold increase and becomes nonmeasurable with the PPMS electronics below ∼70 K. This observation clearly suggests that similar to the As-, Sb-, and Bi-based analogs $BaMn_2P_2$ has an insulating ground state. Additionally, $\rho_{ab}(T)$ data collected at $\mu_0 H = 0$ and 7 T overlap with each other in the entire T range of measurement. This observation suggests that $\mu_0 H \leqslant 7$ T does not have any measurable effect on the interactions and scatterings that dominate the electrical transport within the ab plane of this compound, leading to negligible magnetoresistance. The $\rho_{ab}(T)$ data below $\lesssim$100 K show feature of activated transport [inset(b), Fig. 3] and were fitted using

$$\ln\rho_{ab}(T) = A + \frac{\Delta}{k_B T}, \tag{1}$$

where A is a constant, Δ is activation energy of the band gap, and k_B is Boltzmann constant. The fitted value of $\Delta = 24(2)$ meV suggests it to be a small band gap material. This value is similar to the values reported on a polycrystalline sample of $BaMn_2P_2$ [30] as well as single crystals of $BaMn_2As_2$ and $BaMn_2Sb_2$ (Table I).

C. Heat capacity

The heat capacity at constant pressure C_p versus T data of $BaMn_2P_2$ do not show evidence of any phase transition below room temperature and attain a value of 122.7 J/mol K^2 at 291 K (Fig. 4). This value is close to the Dulong-Petit high-T limit of lattice heat capacity at constant volume given by $C_V = 3nR = 15R = 124.7$ J/mol K^2, where $n = 5$ is the number of atoms per unit cell and R is the gas constant. Attempt to fit the $C_p(T)$ data using Debye model of acoustic phonons [33,34] led to a poor agreement especially at intermediate temperatures. This observation is not surprising as Debye model works well both at low temperatures ($T \ll \Theta_D$) where it predicts a T^3 dependence of C_V and at high temperatures ($T \gtrsim \Theta_D$) where it leads to the Dulong-Petit limit. Here Θ_D is Debye temperature of the material under consideration. However, the model often becomes inconsistent with the experimental results at intermediate temperatures. Often for materials with high Θ_D, one gets a significantly improved fit by incorporating a weighted Einstein single-frequency con-

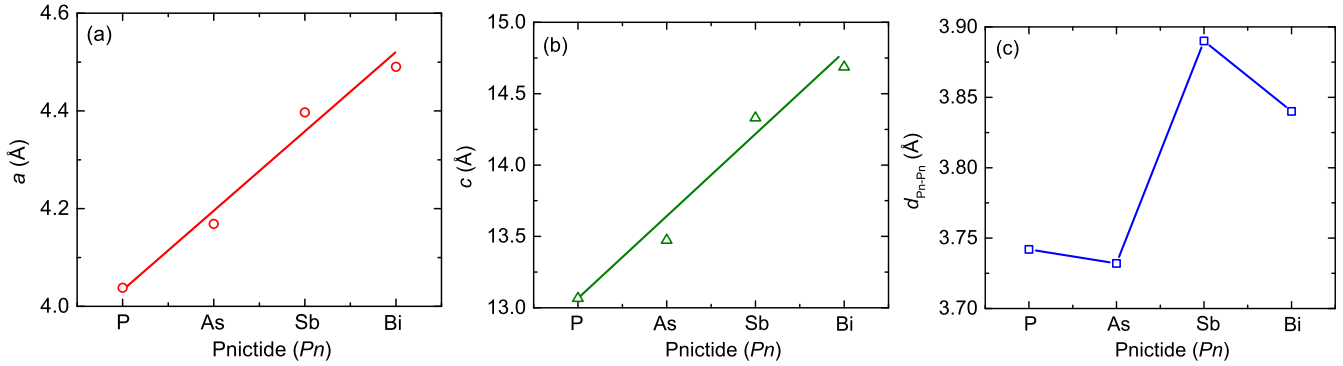


FIG. 2. Variation of tetragonal lattice parameters (a) a, (b) c, and (c) the distance between adjacent pnictogen layers d_{Pn-Pn} in $BaMn_2Pn_2$ (Pn = P, As, Sb, Bi) with the type of pnictide ion present in the unit cell.

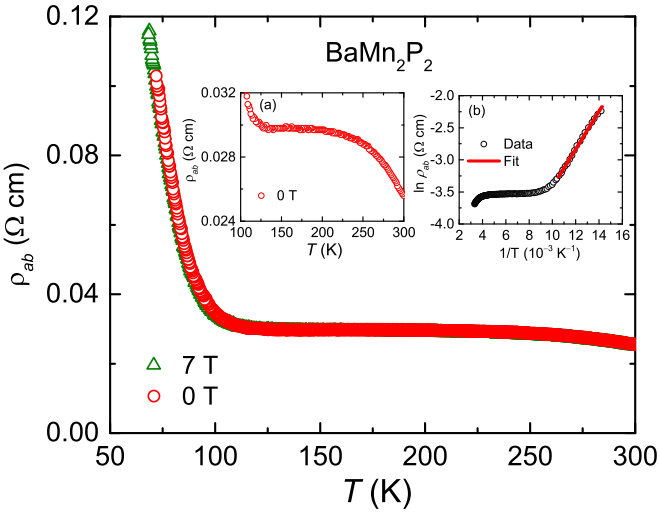


FIG. 3. Electrical resistivity ρ_{ab} vs temperature T of $BaMn_2P_2$ measured at two different applied magnetic fields $\mu_0 H = 0$ and 7 T. Insets (a) $\rho_{ab}(T)$ for $100 \leqslant T \leqslant 300$ K and (b) $\ln\rho_{ab}$ vs T^{-1} along with a linear fit performed for $2\ \text{K} \leqslant T \leqslant 95$ K.

tribution to the Debye model as in

$$C_p(T) = uC_{V\,\text{Debye}}(T) + (1-u)C_{V\,\text{Einstein}}(T), \qquad (2)$$

where $C_{V\,\text{Debye}}(T)$ and $C_{V\,\text{Einstein}}(T)$ are the Debye and Einstein contributions, respectively, and u is fraction of the Debye contribution to the lattice heat capacity [34]. We got a good agreement to the $C_p(T)$ data using Eq. (2) and the fitted value of u, Θ_D, and Einstein temperature Θ_E were 0.324(6), 498(4), and 118(1) K, respectively. As expected, the fitted value of the Θ_D is higher than room temperature.

The low-temperature $C_p(T)$ data were fitted using

$$C_p/T = \gamma + \beta T^2 + \delta T^4, \qquad (3)$$

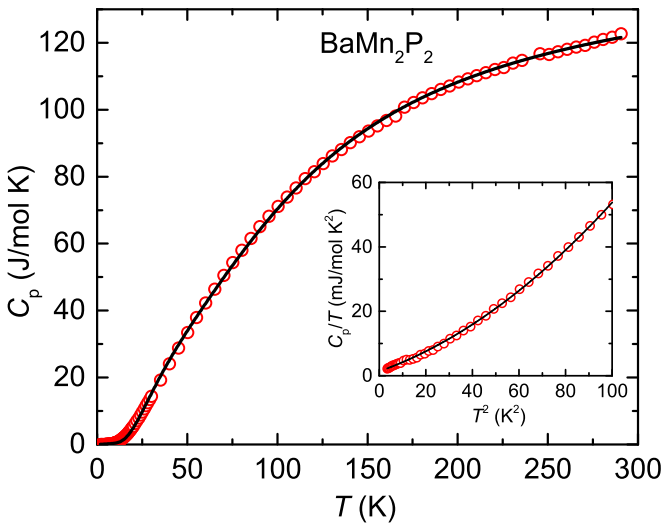


FIG. 4. Heat capacity C_p vs temperature T along with the Debye-Einstein fit as described in the text. Inset: C_p/T vs T^2 data for $T \leqslant 10$ K along with the fit as described in the text.

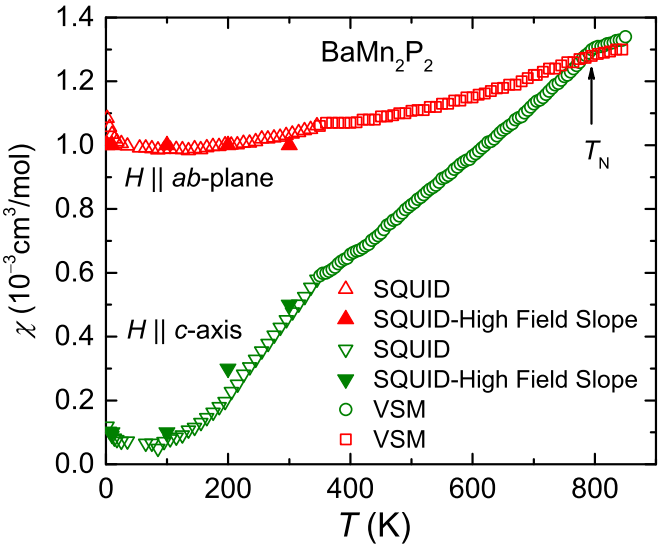


FIG. 5. Anisotropic magnetic susceptibilities $\chi_{ab,c} \equiv M/H$ vs temperature T of $BaMn_2P_2$ measured using a SQUID-magnetometer at $\mu_0 H = 3$ T for $T \leqslant 350$ K, determined from high-field slopes of the isothermal magnetization measurements and measured using a vibrating sample magnetometer for $T \geqslant 350$ K.

where γ is the Sommerfeld electronic heat capacity coefficient while β and δ are the coefficients of low temperature lattice contributions. We obtained a good fit to the low-temperature $C_p(T)$ data using Eq. 3 [inset, Fig. 4] and the fitted values of the parameters are; $\gamma = 0.9(9)$ mJ/mol K^2, $\beta = 0.23(3)$ mJ/mol K^4, and $\delta = 0.0027(1)$ mJ/mol K^6. As expected for a material with insulating ground state, the γ is nearly zero indicating absence of density of states at Fermi level E_F at low temperatures. The low-T Θ_D calculated from the value of β using $\Theta_D = (12\pi^4 Rn/5\beta)^{1/3} = 348(17)$ K is significantly higher than those reported for As-, Sb-, and Bi-counterparts (Table I).

D. Magnetism

Temperature dependence of the magnetic susceptibilities χ_{ab} ($H \parallel ab$ plane) and χ_c ($H \parallel c$ axis) of a crystal of $BaMn_2P_2$ measured at $\mu_0 H = 3$ T are shown in Fig. 5. The $\chi(T)$ data taken using a SQUID magnetometer for $T \leqslant 400$ K and those collected using a PPMS-VSM for $T \geqslant 350$ K connect nearly smoothly, leaving a minor kink at 350 K that likely arises due to slight variation in the orientations of the crystal relative to H when mounted on two different set-ups. The SQUID data are shown up to 350 K for clarity of the figure. The observed T dependence of the anisotropic $\chi_{ab,c}$ data suggests that similar to the As-, Sb-, and Bi-based analog compounds, $BaMn_2P_2$ has a collinear AFM ordering where the localized spins are oriented along the c axis of the tetragonal unit cell. The $T_N = 795(15)$ K deduced from the $\chi_{ab,c}(T)$ data is considerably higher than that observed in the other three materials, suggesting the presence of comparatively stronger magnetic interactions in $BaMn_2P_2$. Further, the $\chi_{ab,c}(T)$ data show a monotonic increase above T_N suggesting the persistence of dynamic short-range quasi-two-dimensional AFM corre-

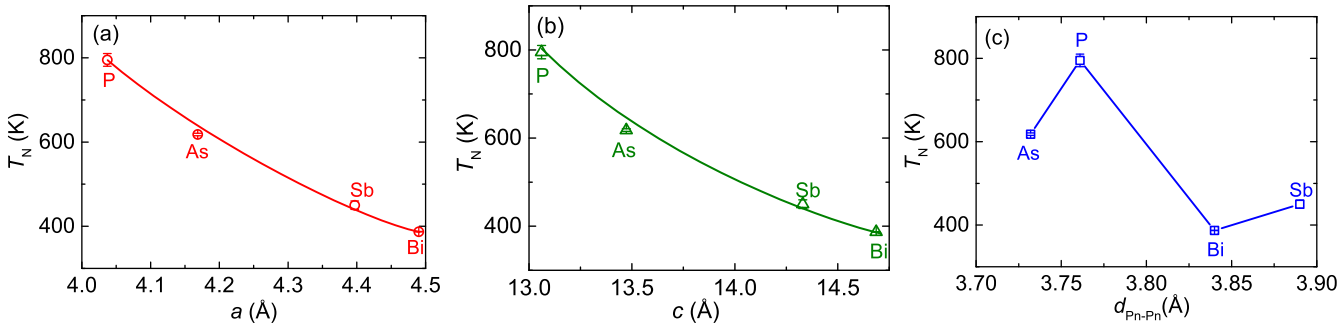


FIG. 6. Variation of antiferromagnetic transition temperature T_N with tetragonal unit cell parameters (a) a, (b) c, and (c) distance between adjacent pnictogen layers d_{Pn-Pn} in $BaMn_2Pn_2$ (Pn = P, As, Sb, Bi).

lations above the ordering temperature, a behavior, which was earlier observed in the other three compounds discussed above. The results show that T_N of $BaMn_2Pn_2$ (Pn = P, As, Sb, Bi) exhibits a monotonic decrease with increase in the tetragonal unit cell parameters a and c [Figs. 6(a) and 6(b)]. This observation infers the progressive weakening of the magnetic interactions operating between the localized Mn spins with increase of the separation between them. While moving from $BaMn_2P_2$ to $BaMn_2Bi_2$ we observe nearly 50% reduction in T_N by approximately 12% increase in the a and c (Table I). Our observations also clearly demonstrate that the T_N values do not have any direct correlation with the d_{Pn-Pn} in these materials [Fig. 6(c)].

Isothermal magnetization M of a single crystal of $BaMn_2P_2$ versus applied magnetic field H for two orientations of the applied field $H \parallel ab$ plane and $H \parallel c$ axis are shown in Figs. 7(a) and 7(b), respectively. As expected for a local-moment AFM system below its ordering temperature, the M is proportional to H for both orientations of the applied field for $T \leqslant 300$ K. The slight nonlinearity in the $M_{ab}(H)$ data at 2 K indicates the presence a very small amount of saturable paramagnetic or FM impurities in the crystal. The same was inferred by the small upturn observed in the $\chi_{ab}(T)$ below ~10 K (Fig. 5). Evidently the effect of these impurities is almost negligible in the T range of our measurements. However, we still attempted to get the intrinsic susceptibilities at low temperatures from the high-field $\mu_0 H \geqslant 4$ T slopes of the $M(H)$ data as shown by the solid symbols in Fig. 5. This observation confirms that the minor upturn in $\chi_{ab}(T)$ below ~10 K is indeed due to the presence of trace saturable impurities.

IV. DISCUSSION

Electrical transport measurements infer an insulating ground state in $BaMn_2P_2$ with activation energy $\Delta = 24(2)$ meV. Similar observations were earlier made on $BaMn_2As_2$ and $BaMn_2Sb_2$ (Table I). The $\rho_{ab}(T)$ of $BaMn_2P_2$ decreases exponentially with the increase of T until ~130 K and then remains nearly T independent up to ~200 K beyond which it decreases slightly with increase of T. This crossover indicates that similar to the As- and Sb-based analogs there is a possibility of the existence of more than one activation energies likely associated with different zones of the elec-

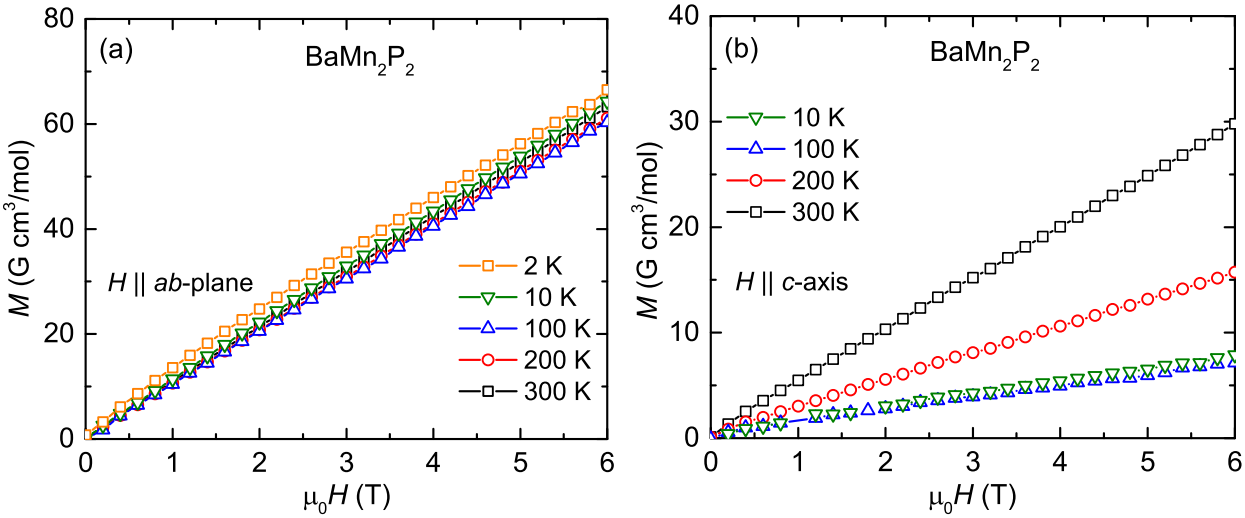


FIG. 7. Isothermal magnetization M vs applied magnetic field H of $BaMn_2P_2$ measured for two different crystal orientations; (a) $H \parallel ab$ plane and (b) $H \parallel c$ axis.

tronic bands dominating the electrical transport in different T regions. The $C_p(T)$ data lead to $\gamma = 0.9(9)$ mJ/mol K^2 corroborating the outcome of the electrical transport measurement and infer an insulating ground state in $BaMn_2P_2$. The Θ_D of $BaMn_2Pn_2$ compounds decreases rapidly with the increase in atomic number of pnictide atom present in the lattice (Table I) inferring that the higher energy modes get enhanced with the inclusion of lighter elements in the lattice.

The insulating ground state of $BaMn_2P_2$ confirms that, similar to other $BaMn_2Pn_2$ compounds, the underlying magnetism in this material is constituted by the localized spins residing on Mn ions. The anisotropic $\chi_{ab,c}(T)$ of $BaMn_2P_2$ clearly show the existence of a collinear AFM with the magnetic easy-axis parallel to the tetragonal c axis and $T_N = 795(15)$ K. The observed T_N in $BaMn_2P_2$ is highest among all the $ThCr_2Si_2$- and $CaAl_2Si_2$-type 122-pnictide compounds reported so far suggesting that the strength of magnetic exchange interactions is strongest in this material. The magnetic interactions within $BaMn_2As_2$ and $BaMn_2Sb_2$ have been successfully explained using J_1-J_2-J_c Heisenberg model of stacked-square lattice, where J_1 and J_2 are the NN and NNN intralayer exchange interactions, respectively, and J_c in the interlayer interaction acting along the c axis [35]. The similarity of the $\chi_{ab,c}(T)$ data of $BaMn_2P_2$ with those of the As-, Sb-, and Bi-analogs [25–27] suggest that magnetic interactions within this material can also be described using the same model. Interestingly, we have observed a monotonic decrease of T_N with the increase in a and c parameters. When moving from $BaMn_2P_2$ to $BaMn_2Bi_2$, about 12% increase in a and c leads to about ∼50% decrease in T_N suggesting a strong dependence of J_1, J_2, and J_c on the intralayer as well as interlayer distances between the localized Mn spins. Further, the $\chi_{ab,c}(T)$ of $BaMn_2P_2$ show a monotonic increase for $T > T_N$. This behavior is similar to what was previously observed in As-, Sb-, and Bi-analogs [26,27,35] and suggests that dynamic short-range quasi-two-dimensional AFM correlations persist above T_N in this material as well.

It is interesting to compare the Mn-based insulating $BaMn_2Pn_2$ compounds with the Co-based metallic ACo_2As_2 (A = Ca, Sr, Ba), which also crystallize in $ThCr_2Si_2$-type structure. ACo_2As_2 compounds exhibit properties that delicately depend upon the interlayer d_{As-As}, which regulates the oxidation state of Co ions in these materials by controlling the extent of the interlayer As-As bonds. As a result, it indirectly controls the magnetic ground state [9]. For example, $BaCo_2As_2$ with $d_{As-As} = 3.78$ Å shows a nonmagnetic ground state [36]. On the other hand, $CaCo_{1.86}As_2$ with $d_{As-As} = 2.73$ Å exhibits an A-type collinear AFM ordering below 52 K [37]. Interestingly, $SrCo_2As_2$ with $d_{As-As} = 3.33$ Å intermediate to those of its Ca and Ba analogs shows no evidence of long-range magnetic ordering, but exhibits stripe-type AFM [10] as well as FM [11] spin fluctuations, where the former is similar to the fluctuations observed in the FeAs-based superconductors. On the contrary, d_{Pn-Pn} does not show any significant variation within the $BaMn_2Pn_2$ compounds and because of the localized nature of d bands it apparently does not have any direct effect on the oxidation state of the Mn ions as well as on the magnetic ground state of these materials. ACo_2As_2 and $BaMn_2Pn_2$ compounds together present a textbook type example of how the structural parameters and electronic band structure can indirectly govern the magnetism within crystalline systems. It is also noteworthy that the ground state crystal structure of AMn_2Pn_2 compounds only depends upon the type of alkaline earth metal present in the lattice while the unit-cell dimensions are controlled by the pnictogen atoms constituting the lattice. This feature could further be used to investigate the structural crossover regions to understand structure-property relationship within this system and to explore instability driven phase transitions and ground states.

As $BaMn_2P_2$ has the highest T_N within this series, it would be very interesting to perform hole-doping studies on this material. A similar investigation in the related compound $BaMn_2As_2$ with $T_N = 618$ K has led to the discovery of a prototype itinerant half-metallic ferromagnetism with $T_c \approx 100$ K. It would be worth to investigate if the stronger exchange interactions resulting in large T_N in $BaMn_2P_2$ can assist in developing a half-metallic FM state with higher T_c. Such investigations would be important as the high-T_c half-metals are desirable candidates for spin-polarized device applications.

V. CONCLUSIONS

High-quality single crystals of $BaMn_2P_2$ were grown using Sn flux. The ab-plane electrical resistivity as well as the heat capacity measurements suggest a small band gap insulating ground state of the material. The anisotropic magnetic susceptibility $\chi_{ab,c}(T)$ measurements show that similar to $BaMn_2Pn_2$ (Pn = As, Sb, Bi) compounds, $BaMn_2P_2$ has a collinear Néel-type AFM ground state with transition temperature $T_N = 795(15)$ K, which is highest among the 122-pnictide compounds investigated so far. The AFM transition temperatures of $BaMn_2Pn_2$ compounds show a monotonic decrease with the increase of tetragonal a and c parameters, where about 12% increase in a and c leads to ∼50% decrease in T_N. These observations suggest a strong dependence of the strength of the magnetic exchange interactions on the separation between the localized spins residing on the Mn ions. The $\chi_{ab,c}(T)$ of $BaMn_2P_2$ show a monotonic increase for $T > T_N$ suggesting the presence of sizable short-range dynamic quasi-two-dimensional AFM correlations above the T_N. Because of the high value of T_N of $BaMn_2P_2$, hole-doping investigations are highly sought for. Similar studies in related $BaMn_2As_2$ with $T_N = 618$ K have led to the discovery of prototypical itinerant half-metallic behavior of the doped holes with $T_c \approx 100$ K. Such investigations become more significant as half-metals with high-T_c are emerging as desirable candidates for spin-polarized transport-based applications.

ACKNOWLEDGMENTS

A.P. acknowledges the financial support from Faculty Research Committee and University Research Committee of the University of the Witwatersrand and National Research Foundation of South Africa. The work at Texas A&M University was supported by the National Science Foundation through Grant No. NSF-DMR-1807451.

[1] Y. Kamihara, T. Watanabe, M. Hirano, and H. Hosono, Iron-Based layered superconductor La[$O_{1-x}F_x$]FeAs ($x = 0.05 - 0.12$) with $T_c = 26$ K, J. Am. Chem. Soc. **130**, 3296 (2008).

[2] C. Wang, L. Li, S. Chi, Z. Zhu, Z. Ren, Y. Li, Y. Wang, X. Lin, Y. Luo, S. Jiang *et al.*, Thorium-doping-induced superconductivity up to 56 K in $Gd_{1-x}Th_xFeAsO$, Europhys. Lett. **83**, 67006 (2008).

[3] J. Paglione and R. L. Greene, High-temperature superconductivity in iron-based materials, Nat. Phys. **6**, 645 (2010).

[4] D. C. Johnston, The puzzle of high temperature superconductivity in layered iron pnictides and chalcogenides, Adv. Phys. **59**, 803 (2010).

[5] G. R. Stewart, Superconductivity in iron compounds, Rev. Mod. Phys. **83**, 1589 (2011).

[6] A. Pandey, B. G. Ueland, S. Yeninas, A. Kreyssig, A. Sapkota, Y. Zhao, J. S. Helton, J. W. Lynn, R. J. McQueeney, Y. Furukawa, A. I. Goldman, and D. C. Johnston, Coexistence of Half-Metallic Itinerant Ferromagnetism with Local-Moment Antiferromagnetism in $Ba_{0.6}K_{0.4}Mn_2As_2$, Phys. Rev. Lett. **111**, 047001 (2013).

[7] B. G. Ueland, A. Pandey, Y. Lee, A. Sapkota, Y. Choi, D. Haskel, R. A. Rosenberg, J. C. Lang, B. N. Harmon, D. C. Johnston, A. Kreyssig, and A. I. Goldman, Itinerant Ferromagnetism in the As-4p Conduction Band of $Ba_{0.6}K_{0.4}Mn_2As_2$ Identified by X-Ray Magnetic Circular Dichroism, Phys. Rev. Lett. **114**, 217001 (2015).

[8] A. Pandey and D. C. Johnston, $Ba_{0.4}Rb_{0.6}Mn_2As_2$: A prototype half-metallic ferromagnet, Phys. Rev. B **92**, 174401 (2015).

[9] A. Pandey, D. G. Quirinale, W. Jayasekara, A. Sapkota, M. G. Kim, R. S. Dhaka, Y. Lee, T. W. Heitmann, P. W. Stephens, V. Ogloblichev, A. Kreyssig, R. J. McQueeney, A. I. Goldman, A. Kaminski, B. N. Harmon, Y. Furukawa, and D. C. Johnston, Crystallographic, electronic, thermal, and magnetic properties of single-crystal $SrCo_2As_2$, Phys. Rev. B **88**, 014526 (2013).

[10] W. Jayasekara, Y. Lee, A. Pandey, G. S. Tucker, A. Sapkota, J. Lamsal, S. Calder, D. L. Abernathy, J. L. Niedziela, B. N. Harmon, A. Kreyssig, D. Vaknin, D. C. Johnston, A. I. Goldman, and R. J. McQueeney, Stripe Antiferromagnetic Spin Fluctuations in $SrCo_2As_2$, Phys. Rev. Lett. **111**, 157001 (2013).

[11] Y. Li, Z. Yin, Z. Liu, W. Wang, Z. Xu, Y. Song, L. Tian, Y. Huang, D. Shen, D. L. Abernathy, J. L. Niedziela, R. A. Ewings, T. G. Perring, D. M. Pajerowski, M. Matsuda, P. Bourges, E. Mechthild, Y. Su, and P. Dai, Coexistence of Ferromagnetic and Stripe Antiferromagnetic Spin Fluctuations in $SrCo_2As_2$, Phys. Rev. Lett. **122**, 117204 (2019).

[12] A. Sapkota, B. G. Ueland, V. K. Anand, N. S. Sangeetha, D. L. Abernathy, M. B. Stone, J. L Niedziela, D. C. Johnston, A. Kreyssig, A. I. Goldman, and R. J. McQueeney, Effective One-Dimensional Coupling in the Highly Frustrated Square-Lattice Itinerant Magnet $CaCo_{2-y}As_2$, Phys. Rev. Lett. **119**, 147201 (2017).

[13] V. K. Anand, H. Kim, M. A. Tanatar, R. Prozorov, and D. C. Johnston, Superconducting and normal-state properties of APd_2As_2 (A = Ca, Sr, Ba) single crystals, Phys. Rev. B **87**, 224510 (2013).

[14] V. K. Anand, H. Kim, M. A. Tanatar, R. Prozorov, and D. C. Johnston, Superconductivity and physical properties of $CaPd_2Ge_2$ single crystals, J. Phys.: Condens. Matter **26**, 405702 (2014).

[15] X. F. Wang, C. Roncaioli, C. Eckberg, H. Kim, J. Yong, Y. Nakajima, S. R. Saha, P. Y. Zavalij, and J. Paglione, Tunable electronic anisotropy in single-crystal ACr_3As_3 (A = K, Rb) quasi-one-dimensional superconductors, Phys. Rev. B **92**, 020508(R) (2015).

[16] K. Zhao, Q.-G. Mu, B.-B. Ruan, T. Liu, B.-J. Pan, M.-H. Zhou, S. Zhang, G.-F. Chen, and Z.-A. Ren, Synthesis and superconductivity of a novel quasi-one-dimensional ternary molybdenum pnictide $Cs_2Mo_3As_3$, APL Mater. **8**, 031103 (2020).

[17] A. Pandey, S. L. Samal, and D. C. Johnston, $CsMn_4As_3$: A Layered tetragonal transition-metal pnictide compound with an antiferromagnetic ground state, Inorg. Chem. **57**, 3206 (2018).

[18] K.-K. Huynh, T. Ogasawara, K. Kitahara, Y. Tanabe, S. Y. Matsushita, T. Tahara, T. Kida, M. Hagiwara, D. Arčon, and K. Tanigaki, Negative and positive magnetoresistance in the itinerant antiferromagnet $BaMn_2Pn_2$ (Pn = P, As, Sb, and Bi), Phys. Rev. B **99**, 195111 (2019).

[19] T. Ogasawara, K.-K. Huynh, T. Tahara, T. Kida, M. Hagiwara, D. Arčon, M. Kimata, S. Y. Matsushita, K. Nagata, and K. Tanigaki, Large negative magnetoresistance in the antiferromagnet $BaMn_2Bi_2$, Phys. Rev. B **103**, 125108 (2021).

[20] T. Ogasawara, K.-K. Huynh, S. Y. Matsushita, M. Kimata, T. Tahara, T. Kida, M. Hagiwara, D. Arčon, and K. Tanigaki, Magnetic field induced Anderson localization in the orbital-selective antiferromagnet $BaMn_2Bi_2$, Phys. Rev. B **106**, L041114 (2022).

[21] A. Mewis, AB_2X_2-Compounds with the $CaAl_2Si_2$ Structure, V [1] The crystal structure of $CaMn_2P_2$, $CaMn_2As_2$, $SrMn_2P_2$ and $SrMn_2As_2$, Z. Naturforsch. B **33**, 606 (1978).

[22] G. Cordier and H. Schäfer, New intermetallic compounds in the anti-Ce_2O_2S-structure type, Z. Naturforsch. B **31**, 1459 (1976).

[23] A. Pandey, R. S. Dhaka, J. Lamsal, Y. Lee, V. K. Anand, A. Kreyssig, T. W. Heitmann, R. J. McQueeney, A. I. Goldman, B. N. Harmon, A. Kaminski, and D. C. Johnston, $Ba_{1-x}K_xMn_2As_2$: An Antiferromagnetic Local-Moment Metal, Phys. Rev. Lett. **108**, 087005 (2012).

[24] A. T. Satya, A. Mani, A. Arulraj, N. V. C. Shekar, K. Vinod, C. S. Sundar, and A. Bharathi, Pressure-induced metallization of $BaMn_2As_2$, Phys. Rev. B **84**, 180515(R) (2011).

[25] Y. Singh, A. Ellern, and D. C. Johnston, Magnetic, transport, and thermal properties of single crystals of the layered arsenide $BaMn_2As_2$, Phys. Rev. B **79**, 094519 (2009).

[26] N. S. Sangeetha, V. Smetana, A.-V. Mudring, and D. C. Johnston, Antiferromagnetism in semiconducting $SrMn_2Sb_2$ and $BaMn_2Sb_2$ single crystals, Phys. Rev. B **97**, 014402 (2018).

[27] B. Saparov and A. S. Sefat, Crystals, magnetic and electronic properties of a new $ThCr_2Si_2$-type $BaMn_2Bi_2$ and K-doped compositions, J. Solid State Chem. **204**, 32 (2013).

[28] S. Calder, B. Saparov, H. B. Cao, J. L. Niedziela, M. D. Lumsden, A. S. Sefat, and A. D. Christianson, Magnetic structure and spin excitations in $BaMn_2Bi_2$, Phys. Rev. B **89**, 064417 (2014).

[29] S. L. Brock, J. E. Greedan, and S. M. Kauzlarich, A test of the application of extended Hückel calculations to the $ThCr_2Si_2$ and $CaAl_2Si_2$ structure types: The case of $SrMn_2P_2$ and $BaMn_2P_2$, J. Solid State Chem. **109**, 416 (1994).

[30] S. L. Brock, J. E. Greedan, and S. M. Kauzlarich, Resistivity and magnetism of AMn_2P_2 (A = Sr, Ba): The effect of structure type on physical properties, J. Solid State Chem. **113**, 303 (1994).

[31] P. C. Canfield, New materials physics, Rep. Prog. Phys. **83**, 016501 (2020).

[32] J. Rodríguez-Carvajal, Recent advances in magnetic structure determination by neutron powder diffraction, Phys. B: Condens. Matter **192**, 55 (1993); see also www.ill.eu/sites/fullprof/.

[33] R. J. Goetsch, V. K. Anand, A. Pandey, and D. C. Johnston, Structural, thermal, magnetic, and electronic transport properties of the $LaNi_2(Ge_{1-x}Px)_2$ system, Phys. Rev. B **85**, 054517 (2012).

[34] E. S. R. Gopal, *Specific Heats at Low Temperatures* (Plenum, New York, 1966).

[35] D. C. Johnston, R. J. McQueeney, B. Lake, A. Honecker, M. E. Zhitomirsky, R. Nath, Y. Furukawa, V. P. Antropov, and Yogesh Singh, Magnetic exchange interactions in $BaMn_2As_2$: A case study of the J_1-J_2-J_c Heisenberg model, Phys. Rev. B **84**, 094445 (2011).

[36] V. K. Anand, D. G. Quirinale, Y. Lee, B. N. Harmon, Y. Furukawa, V. V. Ogloblichev, A. Huq, D. L. Abernathy, P. W. Stephens, R. J. McQueeney, A. Kreyssig, A. I. Goldman, and D. C. Johnston, Crystallography and physical properties of $BaCo_2As_2$, $Ba_{0.94}K_{0.06}Co_2As_2$, and $Ba_{0.78}K_{0.22}Co_2As_2$, Phys. Rev. B **90**, 064517 (2014).

[37] V. K. Anand, R. S. Dhaka, Y. Lee, B. N. Harmon, A. Kaminski, and D. C. Johnston, Physical properties of metallic antiferromagnetic $CaCo_{1.86}As_2$ single crystals, Phys. Rev. B **89**, 214409 (2014).